Supporting Information for

Atmospheric evolution of environmentally persistent free radicals in rural North China Plain: insights into water solubility and effects on $PM_{2.5}$ oxidative potential

Xu Yang[1], Fobang Liu[1,*], Shuqi Yang[1], Yuling Yang[2], Yanan Wang[1], JingJing Li[2], Mingyu Zhao[2], Zhao Wang[1,3], Kai Wang[2], Chi He[1], Haijie Tong[4,*]

[1]Department of Environmental Science and Engineering, School of Energy and Power Engineering, Xi'an Jiaotong University, Xi'an, Shaanxi 710049, China

[2]State Key Laboratory of Nutrient Use and Management, College of Resources and Environmental Sciences, National Academy of Agriculture Green Development, National Observation and Research Station of Agriculture Green Development (Quzhou, Hebei), China Agricultural University, Beijing 100193, China

[3]Shaanxi Provincial Land Engineering Construction Group Co., Ltd., Xi'an, Shaanxi 710075, China.

[4]Institute of Surface Science, Helmholtz-Zentrum Hereon, Max-Planck-Str. 1, Geesthacht 21502, Germany

[*]Corresponding authors: Fobang Liu (fobang.liu@xjtu.edu.cn); Haijie Tong (haijie.tong@hereon.de)

Number of Pages: 30

Number of Texts: 2

Number of Figures: 10

Number of Tables: 10

Text S1: Methods in the quantification of PM oxidative potential

OP^{DTT}: In the DTT depletion assay, the PM filters were first extracted using phosphate-buffered saline (PBS, pH = 7.4) at 2400 rpm for 30 min. The extracts were then adjusted to a final concentration of 100 μg/mL for each sample to account for a non-linear effect. The PM extract was mixed with DTT (100 μM in PBS, Sigma-Aldrich) and incubated at 37 °C for 30 min. At 5 min intervals, 200 μL of the mixture was transferred to react with 5, 5-dithiobis (2-nitrobenzoic acid) (DTNB, 0.24 mM, Sigma-Aldrich) and tris buffer (6.45 mM with 20 mM ethylenediaminetetraacetic acid (EDTA)). The absorbance of the reaction mixture at 412 nm was measured using a microplate reader (SuPerMax 3000FA, Shanghai Flash Spectrum). To obtain the actual DTT consumption, the absorbance of matrix absorbance (PM and matrix) was subtracted from the final absorbance. Additionally, the DTT loss in the filter blank was also subtracted from the DTT loss in the samples. All the steps were performed in dark conditions.

The OP^{DTT} is calculated based on the residual DTT concentration in the samples at different time intervals, i.e., calculated by the slope and intercept of the linear regression of the measured absorbance against time (Fang et al., 2015). Note that both total OP (Total-OP) and water-soluble OP (WS-OP^{DTT}) were determined in this work. For Total-OP^{DTT} determination, unfiltered PM extracts with filter punches left in the extracts were directly mixed with DTT. For WS-OP^{DTT} determination, the extract was filtered through a 0.22 μm PTFE syringe filter before being mixed with DTT. The OP contribution from water-insoluble PM components (WIS-OP^{DTT}) was considered as the difference between Total-OP^{DTT} and WS-OP^{DTT}

$OP^{\bullet OH}$: In the •OH production assay, a fluorescence-based method was used to measure •OH generated by PM. The same extraction method as for the OP measurement was used and a final concentration of PM extract was obtained. Then, 10 mM terephthalate (TPT, Thermo Scientific) and 200 μM ascorbic acid (Sigma-Aldrich) in PBS were added into the PM extract and incubated at 37 °C for 120 min. The added TPT reacted with the generated •OH to form stable and strongly fluorescent hydroxyterephthalic acid (2-OHTA). At specified time intervals (0, 30, 60, 70, 90, 120 min), 200 μL of the mixture was transferred and mixed with 100 μL of dimethyl sulfoxide (100 mM in PBS) to quench the •OH formation (Son et al., 2015). The fluorescent product 2-OHTA was detected at an excitation/emission wavelength of 310/425 nm using a microplate reader (SuPerMax 3000FA, Shanghai Flash Spectrum).

The actual •OH generation rate was determined by subtracting the possible fluorescence from PM and matrix from the final fluorescence. Moreover, the •OH generation by the filter blank was also corrected. The •OH generation rate was calculated based on the determined 2-OHTA concentration at different time intervals as the formation of 2-OHTA is proportional to the generation of •OH. Calibration with 2-OHTA standard (TCI) at concentrations of 0, 2, 3, 4, 5, and 6 μM was performed daily to quantify the formed 2-OHTA concentrations. The •OH concentration was then calculated by the following equation (1):

$$[\bullet\ \mathrm{OH}] = [2-\mathrm{OHTA}]/y_{2-\mathrm{OHTA}}, \quad (1)$$

where [2-OHTA] is the measured concentration of 2-OHTA, $y_{2-\mathrm{OHTA}}$ is the molar yield of 2-OHTA from the reaction of •OH with TPT in PBS, which is 0.35 at pH 7.2 (Li et al., 2019).

Similar to OP measurements, both the •OH generation rate by total PM (Total-$OP^{\bullet OH}$) and water-soluble PM components (WS-$OP^{\bullet OH}$) were determined, and the same extraction method as for OP measurements was used. The •OH generation from water-insoluble PM components (WIS-$OP^{\bullet OH}$) was considered as the difference between Total-$OP^{\bullet OH}$ andWS-$OP^{\bullet OH}$.

Text S2: Discussion of OP_v and OP_m in this work and the literature

Table S3 summarizes the OPv and OPm of PM determined by the DTT assay in this work and the literature. Overall, the OPv and OPm in this work are within the range of those previously reported in North China Plain (NCP).(Liu et al., 2018) Compared with other studies in China, the OPv for this work was found to be lower than Beijing (Lu et al., 2014), Guangzhou (Zhang Man-Man et al., 2019), but higher than Xi'an (Wang et al., 2020b), Shanghai (Lyu et al., 2018), and Nanjing (Ma et al., 2021). In addition, for this study the OPm was lower than in other regions except Xi'an and Guangzhou, and these results suggest that there is a significant spatial variation in OP^{DTT} in Chinese cities.

Comparison with OP from several locations around the globe found that OPv and OPm measured in this work were higher than in Europe and the United States (Chirizzi et al., 2017; Gao et al., 2017; Clemente et al., 2023). but lower than in India and Thailand (Puthussery et al., 2020; Wang et al., 2020a). This may be attributed to the fact that India and Thailand are densely populated and heavily polluted with PM, whereas the air in Europe and the United States is relatively clean. It should be noted that the measured OP^{DTT} varied depending on the extraction method (extraction solvent and extraction time) and filtration matrix (quartz, polytetrafluoroethylene, or mixed cellulose ester), and the OP^{DTT} showed a bimodal distribution due to the variation in particle size also, which may be attributed to the particle size distribution characteristics of carbonaceous, metals.

Table S4 summarizes the OPv and OPm of PM quantified by •OH in this work and in the literature. Overall, the $OP^{\bullet OH}$ measured in this study is lower but in the same order of magnitude when compared to the $OP^{\bullet OH}$ of Beijing and Wangdu in China (Li et al., 2019). It is worth noting that Beijing, Wangdu, and this study were conducted in the North China Plain, but there were significant differences between the three, indicating that there are obvious spatial differences in $OP^{\bullet OH}$ in the North China Plain, which may be due to the different pollution sources in different places. Meanwhile, the OPm results in this study are only higher than those of Pakistan in the United States when compared to foreign countries, suggesting that the study area contains less redox material per unit mass of PM, which may be related to the fact that the study area is rural and there are no obvious sources of pollution emissions in the surrounding area.

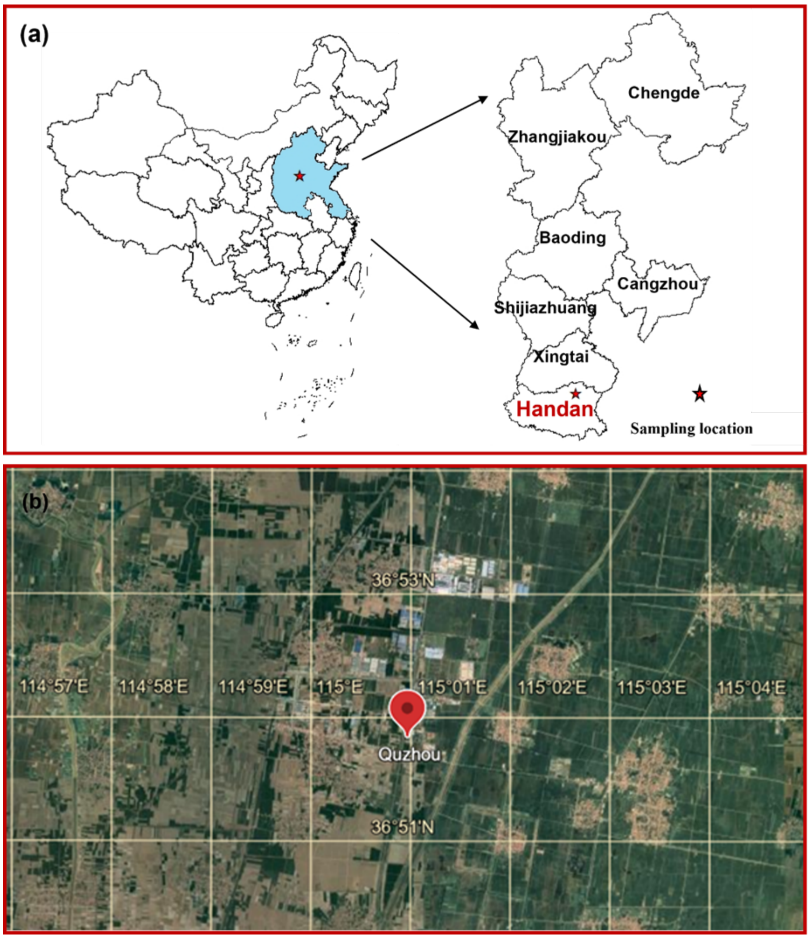

Figure S1. The location of the sampling site. (a) The Quzhou County site (the red star) in the North China Plain; (b) Specific location of the sampling site (from © Google Maps).

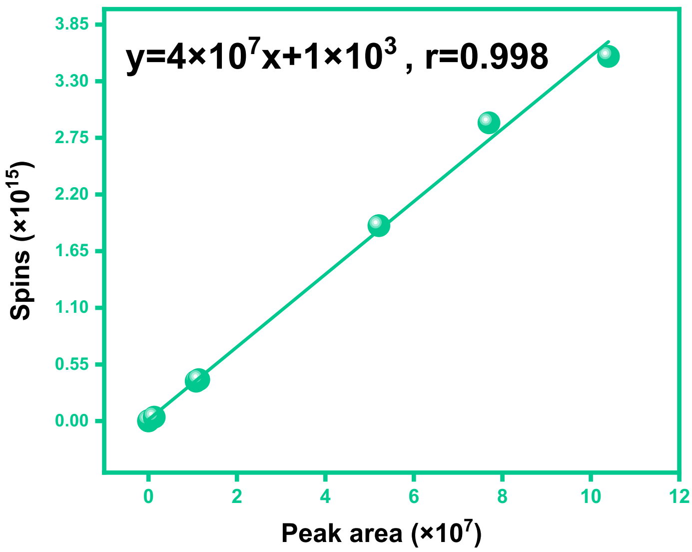

Figure S2. Calibration curve determined by peak area and spins of 4-hydroxy-2,2,6,6-tetramethylpiperidin-1-oxyl (TEMPOL).

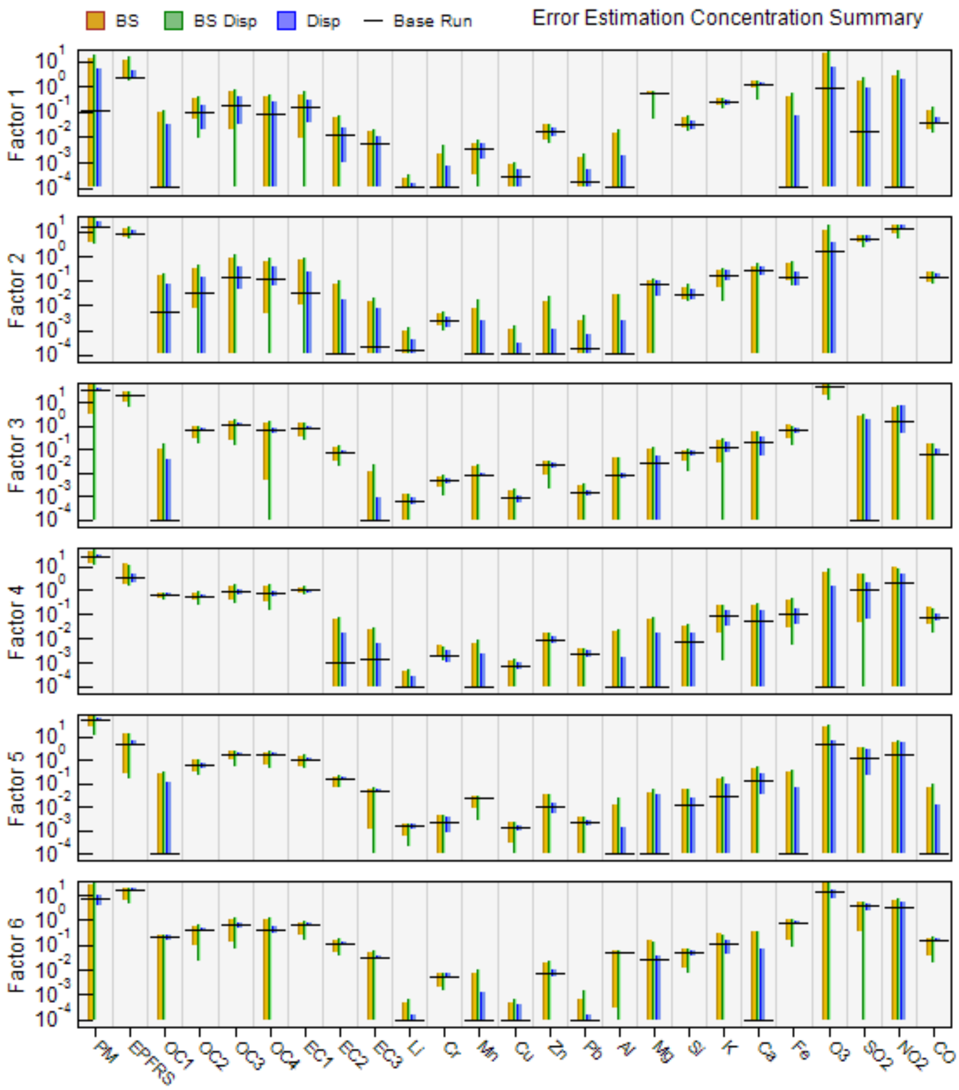

Figure S3. Summary of base run and error estimates as outputted by the PMF analysis.

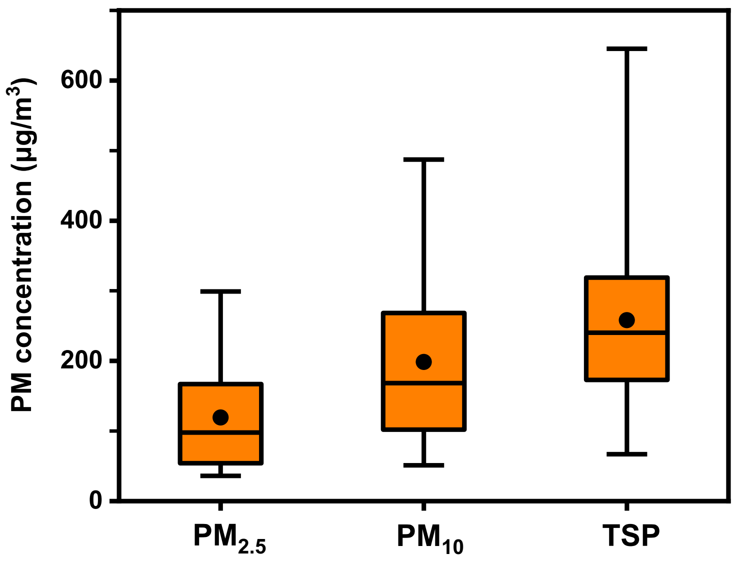

Figure S4. Box plots of PM concentrations in different particle sizes. The boxes represent the 25th percentile (lower edge), median (solid line), mean (solid dot), and 75th percentile (upper edge). The whiskers represent the minimum and maximum.

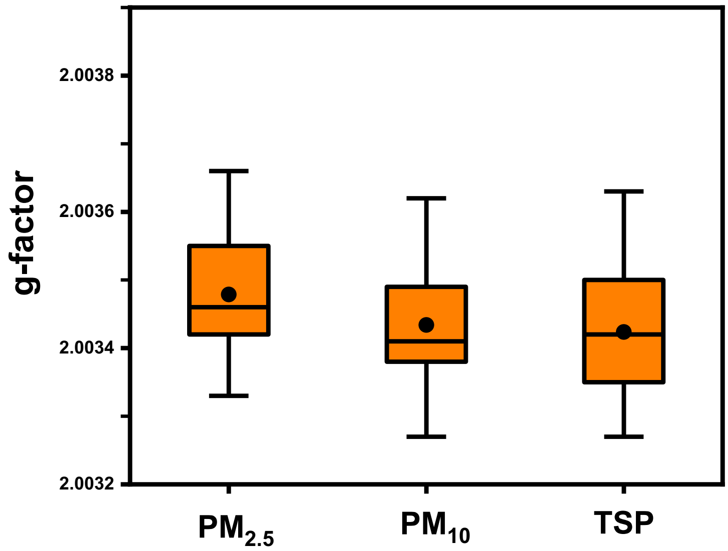

Figure S5. Box plots of variations of g-factor in different particle sizes. The boxes represent the 25th percentile (lower edge), median (solid line), mean (solid dot), and 75th percentile (upper edge). The whiskers represent the minimum and maximum.

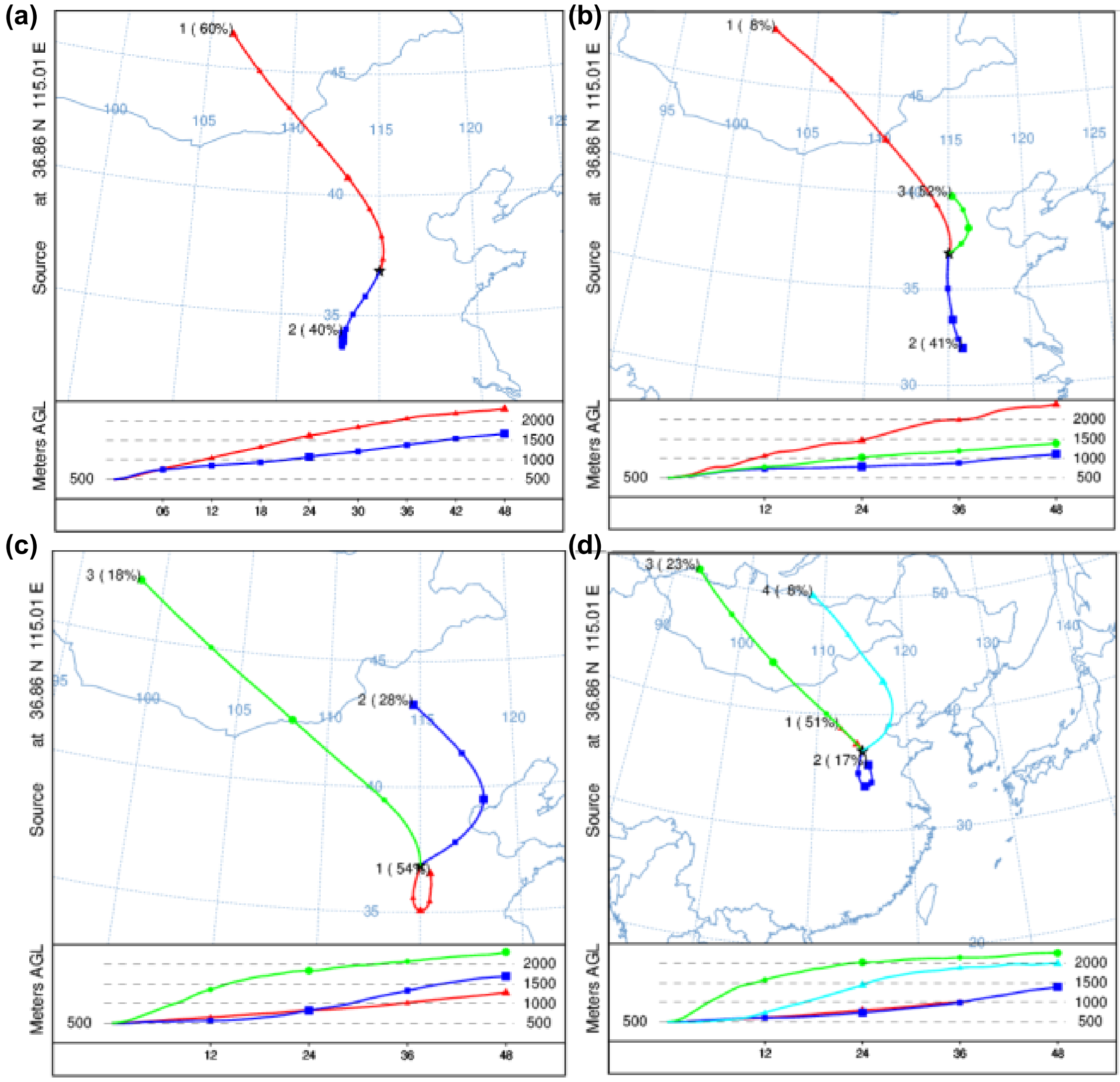

Figure S6. The 48-hr backward trajectory clusters by HYSPLIT for (a) spring; (b) summer; (c) autumn and (d) winter.

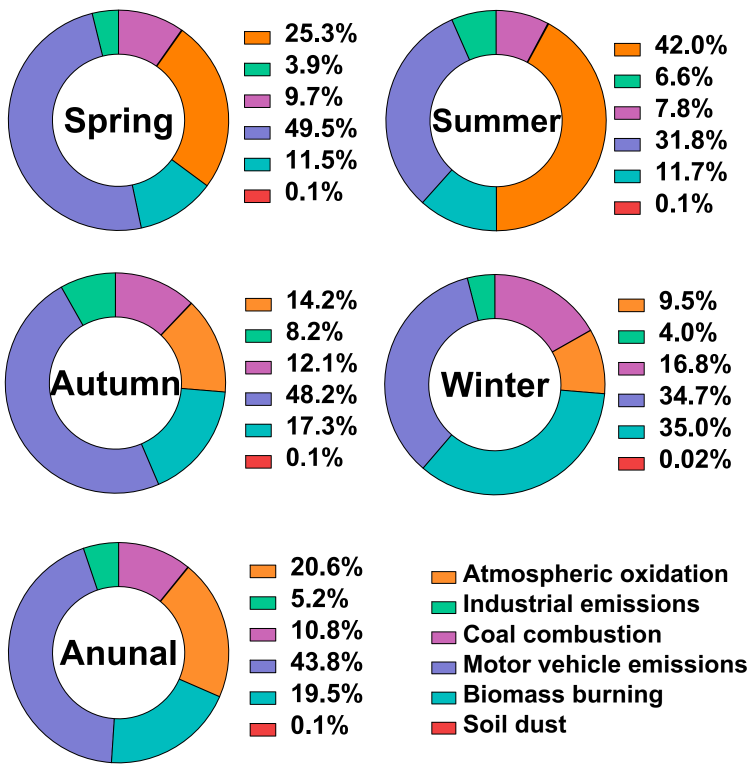

Figure S7. Seasonal and annual contributions of the six factors to PM.

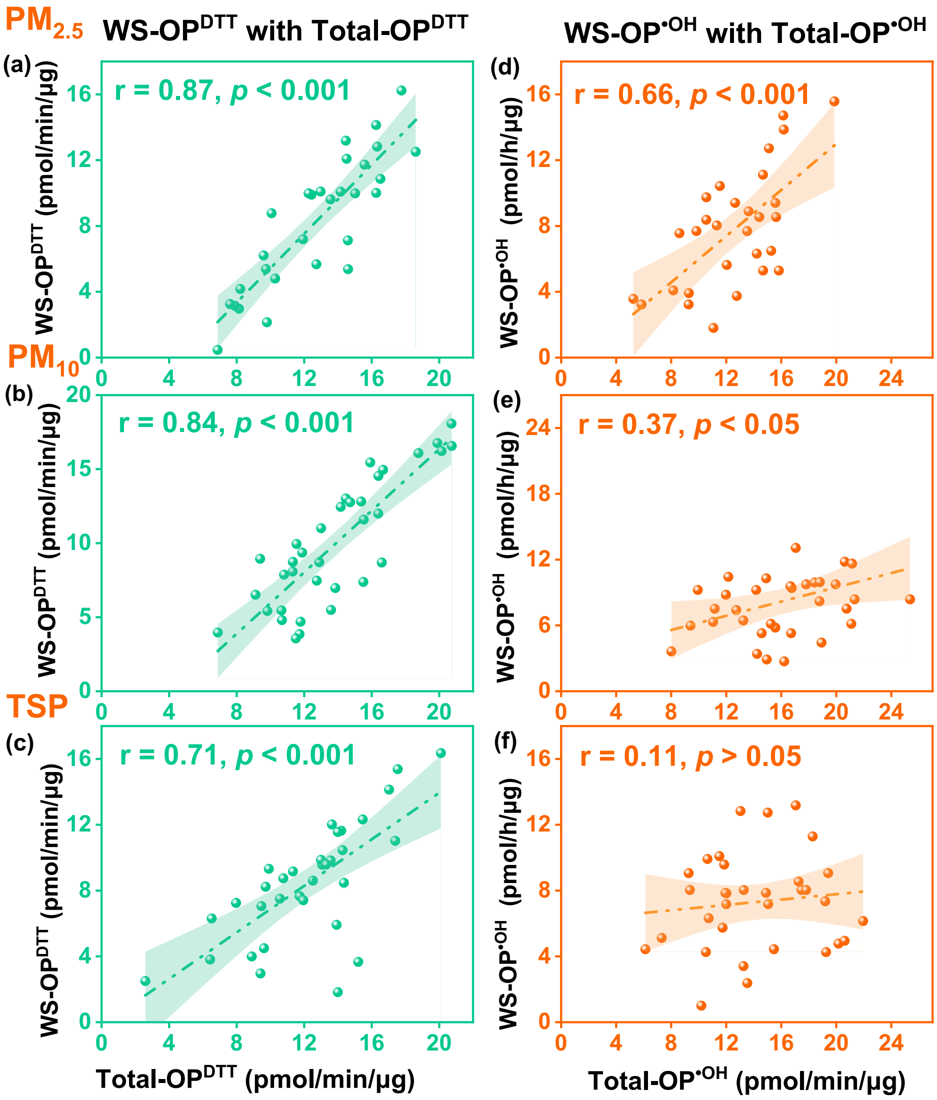

Figure S8. Correlations between WS-OP and Total-OP in different particle sizes; (a-c) Total-OP^{DTT} with WS-OP^{DTT}; (d-f) Total-$OP^{\bullet OH}$ with WS-$OP^{\bullet OH}$. The Pearson correlation coefficients (r) and associated p values are illustrated in the figure. The lines and shadow areas are linear regressions with their 95% confidence intervals.

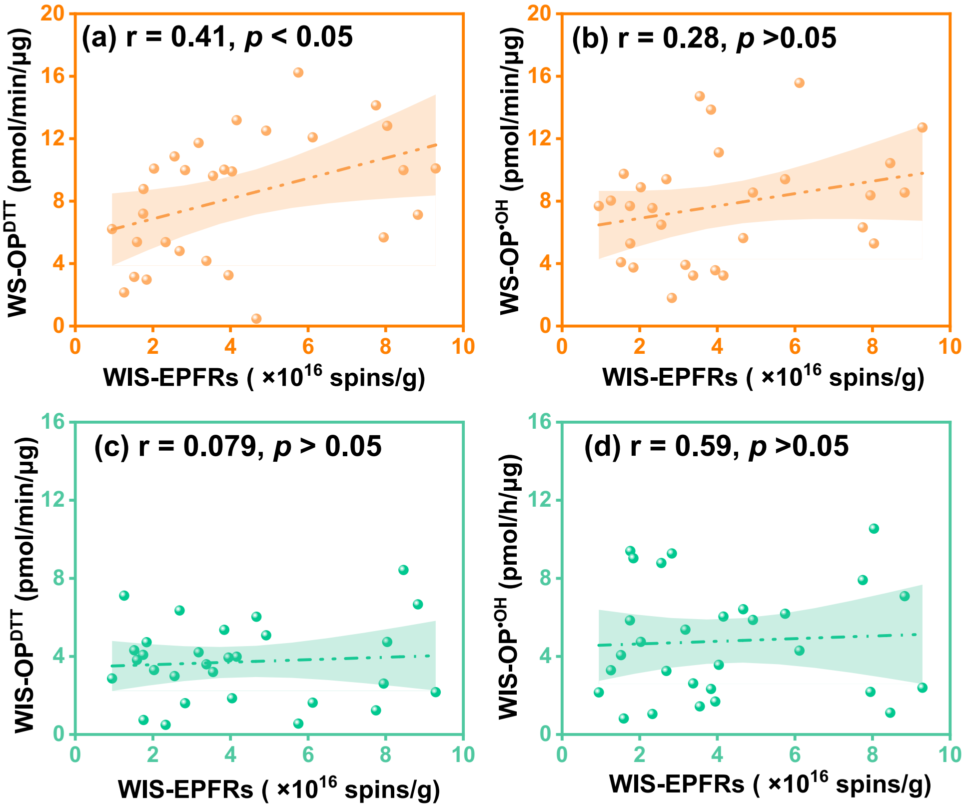

Figure S9. Correlations between WIS-EPFRs and OP; (a-b) WIS-EPFRs with OP_{WS}; (c-d) WIS-EPFRs with OP_{WIS}. The Pearson correlation coefficients (r) and associated *p* values are illustrated in the figure. The lines and shadow areas are linear regressions with their 95% confidence intervals.

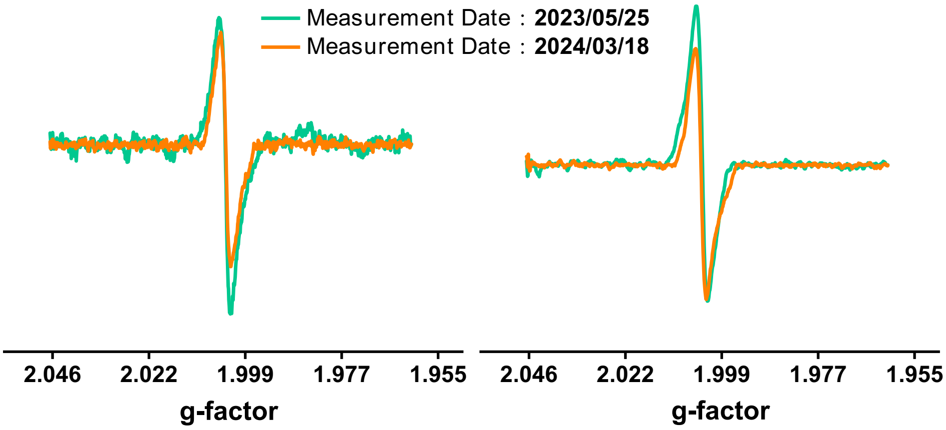

Figure S10. EPR spectra of two randomly selected $PM_{2.5}$ samples were measured on 25 May 2023 and 18 March 2024, showing the stability of the EPFRs.

Table S1. Detailed information on the number of different size PM samples in each season

Season	Particle size	Number
Spring	$PM_{2.5}$	7
	PM_{10}	8
	TSP	8
Summer	$PM_{2.5}$	8
	PM_{10}	9
	TSP	9
Autumn	$PM_{2.5}$	8
	PM_{10}	9
	TSP	9
Winter	$PM_{2.5}$	6
	PM_{10}	7
	TSP	7

Table S2. Comparison of EPFRs in this work and the literature

Location	Type	Site type	Sampling period	PM size	EPFRm (spins/g)	EPFRv (spins/m^3)	References
Quzhou, China	Rural	Villager	2022.04 - 2023.03	$PM_{2.5}$	$6.48 \pm 3.53 \times 10^{16}$	$5.55 \pm 1.05 \times 10^{12}$	This study
				PM_{10}	$3.91 \pm 2.13 \times 10^{16}$	$5.83 \pm 1.04 \times 10^{12}$	
				TSP	$2.96 \pm 1.68 \times 10^{16}$	$5.85 \pm 1.07 \times 10^{12}$	
Harbin, China	Urban	Residential, traffic, commercial	Non-heating season, 2020	Different size		4.58×10^{12}	Jia et al. (2023)
			Heating season, 2020			1.75×10^{14}	
Chongqing, China	Urban	Residential, traffic	Spring, 2017	$PM_{2.5}$	2.83×10^{18}	6.5×10^{13}	Qian et al. (2020)
			Summer, 2017		3.54×10^{18}	4.8×10^{13}	
			Autumn, 2017		2.50×10^{18}	8.4×10^{13}	
			Winter, 2017		1.90×10^{18}	8.1×10^{13}	
Nanjing, China	Urban	Residential, commercial	2019.03 - 2019.05	$PM_{2.5}$	$1.16 - 10.8 \times 10^{16}$	7.61×10^{12}	Guo et al. (2020)
Xi'an, China	Urban	Residential	Spring, 2017	$PM_{2.5}$	3.71×10^{15}	1.65×10^{14}	Wang et al. (2019)
			Summer, 2017		3.19×10^{15}	9.52×10^{13}	
			Autumn, 2017		1.92×10^{15}	1.04×10^{14}	
			Winter, 2017		1.84×10^{15}	1.79×10^{14}	
Yuncheng, China	Urban	Residential	Non-heating season, 2020	$PM_{2.5}$		12.7×10^{12}	Ai et al. (2023)
			Heating season, 2020			28.2×10^{12}	
Beijing, China	Urban	Residential	Non-heating season, 2020	$PM_{2.5}$		16.2×10^{12}	
			Heating season, 2020			14.2×10^{12}	
Beijing, China	Urban	Residential	2016.11-2016.12	TSP	$0.31- 6.2 \times 10^{20}$	$1.6 - 4.5 \times 10^{16}$	Yang et al. (2017)
				$PM<1$	$0.74 -3.9 \times 10^{20}$	$2.7 - 3.5 \times 10^{16}$	
				$PM_{1.0–2.5}$	$0.47 - 6.5 \times 10^{20}$	$0.29 - 1.4 \times 10^{16}$	

				$PM_{2.5-10}$	ND - 8.2 × 10^{19}	0.51 - 2.2 × 10^{15}	
Lahore, Pakistan	Urban	Residential	Summer, 2019	$PM_{2.5}$	2.3 × 10^{17}	1.7 × 10^{13}	Ahmad et al. (2023)
			Winter, 2019		1.1 × 10^{17}	1.2 × 10^{14}	
Louisiana, US	Urban		2008.10 - 2011.10	$PM_{2.5}$	0.20 - 34.8 × 10^{17}		Gehling and Dellinger (2013)
Saudi, Arabia	Urban	Industrial, residential, and traffic	2011.10-2012.06	$PM_{2.5}$	1.6 - 5.8 × 10^{16}		Shaltout et al. (2015)
US	Urban	Five sites		$PM_{2.5}$	0.13 - 1.5 × 10^{17}		Squadrito et al. (2001)
Mainz, German	Suburban	Residential	2015.05-2015.07	Different size	0.68 - 69.5 × 10^{16}		Arangio et al. (2016)

Table S3. The oxidative potential (OP) of PM determined by DTT assay in this work and the literature

Location	Type	Site type	Sampling period	PM size	Determined OP type	OP_v (nmol/min/m^3)	OP_m (pmol/min/μg)	References
Quzhou, China	Rural		2022.04 - 2023.03	$PM_{2.5}$	Total	1.35 ± 0.74	12.23 ± 3.18	This study
					Water-soluble	0.87 ± 0.51	8.51 ± 4.01	
				PM_{10}	Total	2.78 ± 1.56	14.82± 3.78	
					Water-soluble	1.78 ± 0.97	10.14 ± 4.38	
				TSP	Total	3.10 ± 1.84	12.22 ± 3.60	
					Water-soluble	2.01 ± 1.07	8.44 ± 3.60	
Jinzhou, China	Urban	Educational	2015.05 - 2016.04	$PM_{2.5}$	Water-soluble	4.4 ± 2.6	35 ± 18	Liu et al. (2018)
Tianjin, China	Urban	Commercial				6.8 ± 3.4	49 ± 16	
Yantai, China	Urban	Residential and districts				4.2 ± 2.7	30 ± 16	
Beijing, China	Urban	Educational	2015.05 - 2016.04	$PM_{2.5}$	Water-soluble	12.26 ± 6.82	130 ± 100	Lu et al. (2014)
Nanjing, China	Urban	Residential and plants	2016.03 - 2016.12	$PM_{2.5}$	Water-soluble	1.16	20	Ma et al. (2021)
Shanghai, China	Urban	Educational	Haze periods,	Different size	Water-soluble	0.19	62.3	Lyu et al. (2018)
			Nonaze periods,			0.78	42.3	
Xi'an, China	Urban	Residential	Spring, 2017	$PM_{2.5}$	Water-soluble	0.53	11.72	Wang et al. (2020b)
			Summer, 2017			0.50	15.67	
			Autumn, 2017			0.40	6.94	
			Winter, 2017			0.67	6.89	
Guangzhou, China	Urban	Educational	2017 12 - 2018.01	$PM_{2.5}$	Water-soluble	4.67 ± 1.06	13.47 ± 3.86	Zhang Man-Man et al. (2019)
			2018.04 - 2018.05			4.45 ± 1.02	14.66 ± 4.49	

Lecce, Italy	Urban		2013 - 2016	$PM_{2.5}$	Water-soluble	0.29	10.3	Chirizzi et al. (2017)
				PM_{10}		0.36	13.0	
Atlanta, US	Urban	Educational	2016.07 - 2016.08	$PM_{2.5}$	Water-soluble	0.20 ± 0.04		Gao et al. (2017)
					Total	0.32 ± 0.06		
		roadside			Water-soluble	0.21 ± 0.03		
					Total	0.34 ± 0.05		
Delhi, India	Urban		2015.05 - 2016.06	$PM_{2.5}$	Total	5.23 ± 4.6	29.4 ± 18.48	Puthussery et al. (2020)
Bangkok, Thailand	Urban	Educational	2016.01 - 2017.01	TSP	Water-soluble	2.23 ± 0.61	48.1 ± 20.8	Wang et al. (2020a)
Elche, Spain	Urban		Winter, 2021	PM_{10}	Water-soluble	0.40 ± 0.18	18 ± 8	Clemente et al. (2023)
			Summer, 2021			0.28 ± 0.09	11 ± 4	

Table S4. The oxidative potential (OP) of PM determined by •OH production assay in this work and the literature

Location	Type	Sampling period	PM size	Determined OP type	OP_v (pmol/min/m^3)	OP_m (pmol/h/μg)	References
Quzhou, China	Rural	2022.04 - 2023.03	$PM_{2.5}$	Total	24.3 ± 13.4	12.5 ± 3.36	This study
				Water-soluble	15.1 ± 10.5	7.76 ± 3.59	
			PM_{10}	Total	53.5 ± 34.9	16.0 ± 4.15	
				Water-soluble	25.2 ± 16.7	8.17 ± 3.64	
			TSP	Total	61.5 ± 37.9	14.2 ± 4.06	
				Water-soluble	28.8 ± 16.4	7.30 ± 2.94	
Beijing, China	Urban	2014.06 - 2014.07	$PM_{2.5}$	Water-soluble	24.67	28.8	Li et al. (2019)
Wangdu, China	Suburban		$PM_{2.5}$	Water-soluble	35.93	30.58	
Lahore, Pakistan	Urban	Winter, 2019	$PM_{2.5}$	Water-soluble	52.9	6.08	Ahmad et al. (2023)
		Summer, 2019			33.9	12.52	
Fairbanks, US	Residential area	2022.01 - 2022.02	$PM_{2.5}$	Total	1.40	7.14	Yang et al. (2024)
California, US	Several regions	Summer, 2019	$PM_{2.5}$	Total	3.9 ± 1.3	28.8 ± 6.0	Shen et al. (2022)
		Winter, 2020			6.0 ± 2.2	37.8 ± 7.8	
Delhi, Indian	Educational	2022.9.1 - 2022.9.22	$PM_{2.5}$	Total	6.38 ± 0.67	17.0 ± 3.7	Li et al. (2024)

Table S5. Pearson correlation coefficients for the linear regression analysis between Total-OP and mass fraction of PM species in different PM sizes

	OP^{DTTm}				$OP^{\bullet OHm}$			
	Total Size	$PM_{2.5}$	PM_{10}	TSP	Total Size	$PM_{2.5}$	PM_{10}	TSP
OC	0.510**	0.701**	0.390*	0.421*	0.316**	0.492**	0.189	0.447**
EC	0.551**	0.737**	0.527**	0.453**	0.234*	0.515**	0.084	0.419*
EPFRm	0.297**	0.557**	0.325	0.024	0.001	0.480**	-0.021	-0.192
Li	0.062	0.353	-0.247	0.159	0.06	0.306	-0.312	0.282
Mg	0.225	0.471*	0.36	-0.069	-0.073	0.359	-0.147	-0.301
Al	0.187	0.338	0.193	0.028	0.075	0.324	0.001	0.165
Si	0.233*	0.438*	0.297	-0.017	-0.063	0.384*	-0.029	-0.342
K	0.159	0.285	0.251	-0.043	-0.065	0.24	0.155	-0.326
Ca	0.199	0.289	0.335	-0.029	-0.01	0.351	-0.005	-0.322
Cr	0.300**	0.539**	0.146	0.226	0.061	0.369	0.071	-0.054
Mn	0.199	0.412*	-0.025	0.165	0.044	0.348	-0.364*	0.285
Fe	0.380**	0.618**	0.370*	0.181	0.083	0.474**	-0.008	0.380*
Cu	0.113	0.354	-0.047	0.174	0.108	0.545*	-0.179	0.397*
Zn	0.307**	0.381*	0.319	0.520**	0.104	0.374*	-0.079	0.11
Pb	0.317**	0.389*	0.25	0.295	0.297**	0.530**	-0.037	0.380*

* and ** indicate significant correlation at 0.05 and 0.01 level (two-tailed), respectively.

Table S6. Pearson correlation coefficients for the linear regression analysis between WS-OP and mass fraction of PM species in different PM sizes

	OP^{DTTm}				$OP^{\bullet OHm}$			
	Total Size	$PM_{2.5}$	PM_{10}	TSP	Total Size	$PM_{2.5}$	PM_{10}	TSP
OC	0.343**	0.526**	0.205	0.283	0.281**	0.508**	0.041	0.166
EC	0.449**	0.625**	0.397*	0.420*	0.405**	0.444*	0.388*	0.406*
EPFRm	0.320**	0.550**	0.387*	0.204	0.329**	0.428*	0.355*	0.249
Li	-0.014	0.186	-0.313	0.208	0.149	0.322	-0.011	0.2
Mg	0.302**	0.598**	0.382	0.044	0.239*	0.19	0.400*	0.143
Al	0.249*	0.427*	0.269	0.158	0.216*	0.253	0.235	0.215
Si	0.288**	0.524**	0.381*	0.144	0.267**	0.297	0.428*	0.119
K	0.213*	0.373*	0.306	0.119	0.213*	0.26	0.348*	-0.005
Ca	0.263*	0.429*	0.371*	0.047	0.260*	0.263	0.416*	0.141
Cr	0.300**	0.535**	0.207	0.304	0.165	0.114	0.201	0.288
Mn	0.189	0.343	0.036	0.178	0.14	0.2	0.026	0.265
Fe	0.423**	0.633**	0.430*	0.333	0.275**	0.386*	0.235	0.152
Cu	0.106	0.223	-0.007	0.252	0.148	0.621**	-0.19	0.237
Zn	0.335**	0.442*	0.408*	0.526**	0.183	0.168	0.288	0.311
Pb	0.325**	0.303	0.255	0.411*	0.285**	0.499**	0.063	0.256

* and ** indicate significant correlation at 0.05 and 0.01 level (two-tailed), respectively.

Table S7. Pearson correlation coefficients for the linear regression analysis between WIS-OP and mass fraction of PM species in different PM sizes

	OP^{DTTm}				$OP^{\bullet OHm}$			
	Total Size	$PM_{2.5}$	PM_{10}	TSP	Total Size	$PM_{2.5}$	PM_{10}	TSP
OC	0.203*	0.434**	0.256	0.18	0.08	-0.054	0.145	0.28
EC	0.068	-0.014	0.113	0.043	-0.099	0.057	-0.242	0.107
EPFRm	-0.124	-0.213	-0.208	-0.235	-0.263*	0.035	-0.314	-0.319
Li	0.101	0.185	0.214	0.093	-0.062	-0.041	-0.289	0.118
Mg	-0.181	-0.415	-0.159	-0.137	-0.263*	0.214	-0.474*	-0.358
Al	-0.148	-0.288	-0.202	-0.242	-0.099	0.072	-0.194	0.008
Si	-0.17	-0.35	-0.243	-0.21	-0.275**	0.086	-0.382*	-0.367*
K	-0.125	-0.291	-0.175	-0.233	-0.233*	-0.042	-0.143	-0.276
Ca	-0.165	-0.394	-0.162	-0.257	-0.219*	0.09	-0.349*	-0.364*
Cr	-0.065	-0.211	-0.162	-0.101	-0.073	0.303	-0.103	-0.225
Mn	-0.028	-0.03	-0.113	-0.016	-0.068	0.181	-0.372*	0.082
Fe	-0.156	-0.282	-0.217	-0.199	-0.14	0.081	-0.203	-0.054
Cu	-0.004	0.081	-0.067	-0.11	-0.014	-0.167	-0.011	0.178
Zn	-0.12	-0.275	-0.265	-0.008	-0.046	0.24	-0.321	-0.098
Pb	-0.052	0.01	-0.076	-0.151	0.059	0.004	-0.087	-0.358

* and ** indicate significant correlation at 0.05 and 0.01 level (two-tailed), respectively.

Table S8. EPFRs concentrations (spins/m^3) in original and washed samples and proportion of water-soluble fraction

Date	Particle size	Original samples	Washed samples	Water soluble fraction (%)
2022/04/08	$PM_{2.5}$	5.73E+12	3.67E+12	36.0
2022/04/15	$PM_{2.5}$	7.43E+12	5.28E+12	28.9
2022/04/23	$PM_{2.5}$	6.22E+12	4.15E+12	33.3
2022/05/18	$PM_{2.5}$	1.13E+12	5.17E+11	54.1
2022/06/02	$PM_{2.5}$	6.11E+12	3.76E+12	38.5
2022/06/15	$PM_{2.5}$	6.19E+12	2.07E+12	66.6
2022/06/23	$PM_{2.5}$	4.46E+12	3.39E+12	23.9
2022/07/2	$PM_{2.5}$	1.02E+12	7.30E+11	28.2
2022/07/17	$PM_{2.5}$	5.16E+12	2.91E+12	43.6
2022/07/23	$PM_{2.5}$	2.06E+12	1.11E+12	45.8
2022/08/1	$PM_{2.5}$	2.59E+12	1.44E+12	44.3
2022/08/22	$PM_{2.5}$	3.15E+12	2.34E+12	25.7
2022/09/01	$PM_{2.5}$	3.49E+12	2.61E+12	25.1
2022/09/16	$PM_{2.5}$	6.12E+12	3.46E+12	43.5
2022/09/22	$PM_{2.5}$	4.14E+12	3.73E+12	9.9
2022/10/04	$PM_{2.5}$	9.85E+11	6.17E+11	37.3
2022/10/12	$PM_{2.5}$	1.77E+12	1.33E+12	25.0
2022/10/21	$PM_{2.5}$	1.86E+12	1.23E+12	33.7
2022/11/03	$PM_{2.5}$	7.37E+11	6.14E+11	16.7
2022/11/12	$PM_{2.5}$	7.81E+12	6.77E+12	13.3
2022/12/07	$PM_{2.5}$	4.64E+12	3.32E+12	28.4
2022/12/25	$PM_{2.5}$	3.95E+12	1.86E+12	52.9
2023/01/02	$PM_{2.5}$	7.46E+12	3.34E+12	55.2
2023/01/25	$PM_{2.5}$	9.41E+12	6.21E+12	34.0
2023/02/15	$PM_{2.5}$	7.73E+12	4.36E+12	43.6
2023/02/25	$PM_{2.5}$	8.64E+11	8.16E+11	5.6
2023/03/5	$PM_{2.5}$	1.17E+12	8.05E+11	31.5
2023/03/12	$PM_{2.5}$	1.71E+12	1.30E+12	24.4
2023/03/27	$PM_{2.5}$	3.04E+12	2.37E+12	21.9
2022/04/24	PM_{10}	5.62E+12	4.35E+12	22.6
2023/03/13	PM_{10}	1.82E+12	1.06E+12	41.5
2022/04/17	TSP	1.00E+12	5.69E+11	43.2
2023/03/29	TSP	1.37E+12	5.66E+11	58.8
2022/06/03	PM_{10}	1.39E+12	9.78E+11	29.7
2022/07/18	PM_{10}	4.99E+12	3.22E+12	35.4
2022/06/04	TSP	1.45E+12	8.63E+11	40.5
2022/06/18	TSP	9.73E+12	8.05E+12	17.2
2022/10/22	PM_{10}	1.27E+12	9.55E+11	24.5
2022/11/27	PM_{10}	2.06E+12	1.42E+12	31.4

2022/10/06	TSP	4.73E+12	2.68E+12	43.4
2022/10/24	TSP	1.78E+12	1.10E+12	38.2
2023/01/26	PM_{10}	2.25E+12	1.60E+12	28.9
2023/02/06	PM_{10}	1.65E+12	8.60E+11	47.9
2022/12/27	TSP	2.40E+12	1.07E+12	55.4
2023/02/07	TSP	4.68E+12	2.64E+12	43.6
Average				35.2

Table S9. EPFRs concentrations (spins/m^3) in original and acidified samples and proportion of acid-reduced fraction

Date	Particle size	Original samples	Acidified samples	Acid-reduced fraction (%)
2022/04/08	$PM_{2.5}$	3.99E+12	1.74E+12	56.5
2022/07/23	$PM_{2.5}$	1.51E+12	6.21E+11	58.8
2022/08/22	$PM_{2.5}$	3.16E+12	9.65E+11	69.4
2022/07/17	$PM_{2.5}$	2.28E+12	1.03E+12	54.5
2023/03/05	$PM_{2.5}$	4.49E+12	ND	100
2023/03/12	$PM_{2.5}$	1.86E+12	4.08E+11	78.1
Average				69.6

Table S10. Pearson correlation coefficients between EPFRm and mass fraction of PM species

	Total Size	$PM_{2.5}$	PM_{10}	TSP
OC	0.463**	0.694**	0.133	0.023
EC	0.630**	0.784**	0.284	0.286
Li	0.114	0.249	0.132	0.091
Mg	0.705**	0.658**	0.569**	0.593**
Al	0.575**	0.490**	0.741**	0.420*
Si	0.919**	0.876**	0.936**	0.894**
K	0.774**	0.809**	0.680**	0.308
Ca	0.623**	0.560**	0.614**	0.362*
V	0.843**	0.821**	0.742**	0.804**
Cr	0.793**	0.781**	0.681**	0.693**
Mn	0.348**	0.405*	0.357*	0.078
Fe	0.880**	0.951**	0.814**	0.693**
Cu	0.101	0.269	-0.049	-0.369*
Zn	0.536**	0.489**	0.778**	0.472**
Cd	0.362**	0.532**	0.524**	0.32
Pb	0.187	0.411*	0.117	0.097

* and ** indicate significant correlation at 0.05 and 0.01 level (two-tailed), respectively.

References

Ahmad, M., Chen, J., Yu, Q., Tariq Khan, M., Weqas Ali, S., Nawab, A., Phairuang, W., and Panyametheekul, S.: Characteristics and Risk Assessment of Environmentally Persistent Free Radicals (EPFRs) of PM2.5 in Lahore, Pakistan, International journal of environmental research and public health, 20, 2384, https://doi.org/10.3390/ijerph20032384, 2023.

Ai, J., Qin, W. H., Chen, J., Sun, Y. W., Yu, Q., Xin, K., Huang, H. Y., Zhang, L. Y., Ahmad, M., and Liu, X. A.: Pollution characteristics and light-driven evolution of environmentally persistent free radicals in PM2.5 in two typical northern cities of China, Journal of Hazardous Materials, 454, 131466, https://doi.org/10.1016/j.jhazmat.2023.131466, 2023.

Arangio, A. M., Tong, H. J., Socorro, J., Pöschl, U., and Shiraiwa, M.: Quantification of environmentally persistent free radicals and reactive oxygen species in atmospheric aerosol particles, Atmospheric Chemistry and Physics, 16, 13105-13119, https://doi.org/10.5194/acp-16-13105-2016, 2016.

Chirizzi, D., Cesari, D., Guascito, M. R., Dinoi, A., Giotta, L., Donateo, A., and Contini, D.: Influence of Saharan dust outbreaks and carbon content on oxidative potential of water-soluble fractions of PM2.5 and PM10, Atmospheric Environment, 163, 1-8, https://doi.org/10.1016/j.atmosenv.2017.05.021, 2017.

Clemente, A., Gil-Moltó, J., Yubero, E., Juárez, N., Nicolás, J. F., Crespo, J., and Galindo, N.: Sensitivity of PM10 oxidative potential to aerosol chemical composition at a Mediterranean urban site: ascorbic acid versus dithiothreitol measurements, Air Qual. Atmos. Health, 16, 1165-1172, https://doi.org/10.1007/s11869-023-01332-1, 2023.

Fang, T., Verma, V., Guo, H., King, L. E., and Edgerton, E. S.: A semi-automated system for quantifying the oxidative potential of ambient particles in aqueous extracts using the dithiothreitol (DTT) assay: results from the Southeastern Center for Air Pollution and Epidemiology (SCAPE), Atmos. Meas. Tech., 8, 471-482, https://doi.org/10.5194/amt-8-471-2015, 2015.

Gao, D., Fang, T., Verma, V., Zeng, L. G., and Weber, R. J.: A method for measuring total aerosol oxidative potential (OP) with the dithiothreitol (DTT) assay and comparisons between an urban and roadside site of water-soluble and total OP, Atmos. Meas. Tech., 10, 2821-2835, https://doi.org/10.5194/amt-10-2821-2017, 2017.

Gehling, W. and Dellinger, B.: Environmentally Persistent Free Radicals and Their Lifetimes in PM2.5, Environmental Science & Technology, 47, 8172-8178, https://doi.org/10.1021/es401767m, 2013.

Guo, X. W., Zhang, N., Hu, X., Huang, Y., Ding, Z. H., Chen, Y. J., and Lian, H. Z.: Characteristics and potential inhalation exposure risks of PM2.5-bound environmental persistent free radicals in Nanjing, a mega-city in China, Atmospheric Environment, 224, 117355, https://doi.org/10.1016/j.atmosenv.2020.117355, 2020.

Jia, S.-M., Wang, D.-Q., Liu, L.-Y., Zhang, Z.-F., and Ma, W.-L.: Size-resolved environmentally persistent free radicals in cold region atmosphere: Implications for inhalation exposure risk, Journal of Hazardous Materials, 443, 130263, https://doi.org/10.1016/j.jhazmat.2022.130263, 2023.

Li, C., Hakkim, H., Sinha, V., Sinha, B., Pardo, M., Cai, D., Reicher, N., Chen, J., Hao, K., and Rudich, Y.: Variation of PM2. 5 Redox Potential and Toxicity During Monsoon in Delhi, India, ACS ES&T Air, 1, 316–329, 2024.

Li, X. Y., Kuang, X. B. M., Yan, C. Q., Ma, S. X., Paulson, S. E., Zhu, T., Zhang, Y. H., and Zheng, M.: Oxidative Potential by PM2.5 in the North China Plain: Generation of Hydroxyl Radical, Environmental Science & Technology, 53, 512-520, https://doi.org/10.1021/acs.est.8b05253, 2019.

Liu, W. J., Xu, Y. S., Liu, W. X., Liu, Q. Y., Yu, S. Y., Liu, Y., Wang, X., and Tao, S.: Oxidative potential of ambient PM2.5 in the coastal cities of the Bohai Sea, northern China: Seasonal variation and source apportionment, Environmental Pollution, 236, 514-528, https://doi.org/10.1016/j.envpol.2018.01.116, 2018.

Lu, Y., Su, S., Jin, W. J., Wang, B., Li, N., Shen, H. Z., Li, W., Huang, Y., Chen, H., Zhang, Y. Y., Chen, Y. C., Lin, N., Wang, X. L., and Tao, S.: Characteristics and cellular effects of ambient particulate matter from Beijing, Environmental Pollution, 191, 63-69, https://doi.org/10.1016/j.envpol.2014.04.008, 2014.

Lyu, Y., Guo, H. B., Cheng, T. T., and Li, X.: Particle Size Distributions of Oxidative Potential of Lung-Deposited Particles: Assessing Contributions from Quinones and Water-Soluble Metals, Environmental Science & Technology, 52, 6592-6600, https://doi.org/10.1021/acs.est.7b06686, 2018.

Ma, X. Y., Nie, D. Y., Chen, M. D., Ge, P. X., Liu, Z. J., Ge, X. L., Li, Z. R., and Gu, R.: The Relative Contributions of Different Chemical Components to the Oxidative Potential of Ambient Fine Particles in Nanjing Area, International Journal of Environmental Research and Public Health, 18, https://doi.org/10.3390/ijerph18062789, 2021.

Puthussery, J. V., Singh, A., Rai, P., Bhattu, D., Kumar, V., Vats, P., Furger, M., Rastogi, N., Slowik, J. G., Ganguly, D., Prevot, A. S. H., Tripathi, S. N., and Verma, V.: Real-Time Measurements of PM2.5 Oxidative Potential Using a Dithiothreitol Assay in Delhi, India, Environmental Science & Technology Letters, 7, 504-510, https://doi.org/10.1021/acs.estlett.0c00342, 2020.

Qian, R. Z., Zhang, S. M., Peng, C., Zhang, L. Y., Yang, F. M., Tian, M., Huang, R. J., Wang, Q. Y., Chen, Q. C., Yao, X. J., and Chen, Y.: Characteristics and potential exposure risks of environmentally persistent free radicals in PM2.5 in the three gorges reservoir area, Southwestern China, Chemosphere, 252, 10, https://doi.org/10.1016/j.chemosphere.2020.126425, 2020.

Shaltout, A. A., Boman, J., Shehadeh, Z. F., Al-Malawi, D. A. R., Hemeda, O. M., and Morsy, M. M.: Spectroscopic investigation of PM2.5 collected at industrial, residential and traffic sites in Taif, Saudi Arabia, J. Aerosol. Sci., 79, 97-108, https://doi.org/10.1016/j.jaerosci.2014.09.004, 2015.

Shen, J. Q., Taghvaee, S., La, C., Oroumiyeh, F., Liu, J., Jerrett, M., Weichenthal, S., Del Rosario, I., Shafer, M. M., Ritz, B., Zhu, Y. F., and Paulson, S. E.: Aerosol Oxidative Potential in the Greater Los Angeles Area: Source Apportionment and Associations with Socioeconomic Position, Environmental Science & Technology, 56, 17795-17804, https://doi.org/10.1021/acs.est.2c02788, 2022.

Son, Y., Mishin, V., Welsh, W., Lu, S. E., Laskin, J. D., Kipen, H., and Meng, Q. M.: A Novel High-Throughput Approach to Measure Hydroxyl Radicals Induced by Airborne Particulate Matter, International Journal of Environmental Research and Public Health, 12, 13678-13695, https://doi.org/10.3390/ijerph121113678, 2015.

Squadrito, G. L., Cueto, R., Dellinger, B., and Pryor, W. A.: Quinoid redox cycling as a mechanism for sustained free radical generation by inhaled airborne particulate matter, Free Radical Biology and Medicine, 31, 1132-1138, https://doi.org/10.1016/s0891-5849(01)00703-1, 2001.

Wang, J. Q., Jiang, H. Y., Jiang, H. X., Mo, Y. Z., Geng, X. F., Li, J. B., Mao, S. D., Bualert, S., Ma, S. X., Li, J., and Zhang, G.: Source apportionment of water-soluble oxidative potential in ambient total suspended particulate from Bangkok: Biomass burning versus fossil fuel combustion, Atmospheric Environment, 235, 117624, https://doi.org/10.1016/j.atmosenv.2020.117624, 2020a.

Wang, Y. Q., Li, S. P., Wang, M. M., Sun, H. Y., Mu, Z., Zhang, L. X., Li, Y. G., and Chen, Q. C.: Source apportionment of environmentally persistent free radicals (EPFRs) in PM2.5 over Xi'an, China, Science of the Total Environment, 689, 193-202, https://doi.org/10.1016/j.scitotenv.2019.06.424, 2019.

Wang, Y. Q., Wang, M. M., Li, S. P., Sun, H. Y., Mu, Z., Zhang, L. X., Li, Y. G., and Chen, Q. C.: Study on the oxidation potential of the water-soluble components of ambient PM2.5 over Xi'an, China: Pollution levels, source apportionment and transport pathways, Environment International, 136, 11, https://doi.org/10.1016/j.envint.2020.105515, 2020b.

Yang, L. L., Liu, G. R., Zheng, M. H., Jin, R., Zhu, Q. Q., Zhao, Y. Y., Wu, X. L., and Xu, Y.: Highly Elevated Levels and Particle-Size Distributions of Environmentally Persistent Free Radicals in Haze-Associated

Atmosphere, Environmental Science & Technology, 51, 7936-7944, https://doi.org/10.1021/acs.est.7b01929, 2017.

Yang, Y., Battaglia, M. A., Mohan, M. K., Robinson, E. S., DeCarlo, P. F., Edwards, K. C., Fang, T., Kapur, S., Shiraiwa, M., Cesler-Maloney, M., Simpson, W. R., Campbell, J. R., Nenes, A., Mao, J., and Weber, R. J.: Assessing the Oxidative Potential of Outdoor PM2.5 in Wintertime Fairbanks, Alaska, ACS ES&T air, 1, 175-187, https://doi.org/10.1021/acsestair.3c00066, 2024.

ZHANG Man-man, LI Hui-rong, YANG Wen-da, SUN Jia-yin, and Cheng, W.: Measurement based on DTT method of the PM2.5 oxidative potential in Guangzhou urban area, China Environmental Science 2019.